EXPLAINING EXTREME EVENTS OF 2016

From A Climate Perspective

Special Supplement to the
Bulletin of the American Meteorological Society
Vol. 99, No. 1, January 2018

EXPLAINING EXTREME EVENTS OF 2016 FROM A CLIMATE PERSPECTIVE

Editors

Stephanie C. Herring, Nikolaos Christidis, Andrew Hoell, James P. Kossin,
Carl J. Schreck III, and Peter A. Stott

Special Supplement to the

Bulletin of the American Meteorological Society

Vol. 99, No. 1, January 2018

American Meteorological Society

Corresponding Editor:

Stephanie C. Herring, PhD
NOAA National Centers for Environmental Information
325 Broadway, E/CC23, Rm 1B-131
Boulder, CO 80305-3328
E-mail: stephanie.herring@noaa.gov

Cover credit:

©The Ocean Agency / XL Catlin Seaview Survey / Chrisophe Bailhache—A panoramic image of coral bleaching at Lizard Island on the Great Barrier Reef, captured by The Ocean Agency / XL Catlin Seaview Survey / Christophe Bailhache in March 2016.

HOW TO CITE THIS DOCUMENT

Citing the complete report:

Herring, S. C., N. Christidis, A. Hoell, J. P. Kossin, C. J. Schreck III, and P. A. Stott, Eds., 2018: Explaining Extreme Events of 2016 from a Climate Perspective. *Bull. Amer. Meteor. Soc.*, **99** (1), S1–S157.

Citing a section (example):

Quan, X.W., M. Hoerling, L. Smith, J. Perlwitz, T. Zhang, A. Hoell, K. Wolter, and J. Eischeid, 2018: Extreme California Rains During Winter 2015/16: A Change in El Niño Teleconnection? [in "Explaining Extreme Events of 2016 from a Climate Perspective"]. *Bull. Amer. Meteor. Soc.*, **99** (1), S54–S59, doi:10.1175/BAMS-D-17-0118.1.

EDITORIAL AND PRODUCTION TEAM

Riddle, Deborah B., Lead Graphics Production, NOAA/NESDIS National Centers for Environmental Information, Asheville, NC

Love-Brotak, S. Elizabeth, Graphics Support, NOAA/NESDIS National Centers for Environmental Information, Asheville, NC

Veasey, Sara W., Visual Communications Team Lead, NOAA/NESDIS National Centers for Environmental Information, Asheville, NC

Fulford, Jennifer, Editorial Support, Telesolv Consulting LLC, NOAA/NESDIS National Centers for Environmental Information, Asheville, NC

Griffin, Jessicca, Graphics Support, Cooperative Institute for Climate and Satellites-NC, North Carolina State University, Asheville, NC

Misch, Deborah J., Graphics Support, Telesolv Consulting LLC, NOAA/NESDIS National Centers for Environmental Information, Asheville, NC

Osborne, Susan, Editorial Support, Telesolv Consulting LLC, NOAA/NESDIS National Centers for Environmental Information, Asheville, NC

Sprain, Mara, Editorial Support, LAC Group, NOAA/NESDIS National Centers for Environmental Information, Asheville, NC

Young, Teresa, Graphics Support, Telesolv Consulting LLC, NOAA/NESDIS National Centers for Environmental Information, Asheville, NC

TABLE OF CONTENTS

ABSTRACT—Stephanie C. Herring, Nikolaos Christidi, Andrew Hoell, James P. Kossin, Carl J. Schreck III, and Peter A. Stott

This sixth edition of explaining extreme events of the previous year (2016) from a climate perspective is the first of these reports to find that some extreme events were not possible in a preindustrial climate. The events were the 2016 record global heat, the heat across Asia, as well as a marine heat wave off the coast of Alaska. While these results are novel, they were not unexpected. Climate attribution scientists have been predicting that eventually the influence of human-caused climate change would become sufficiently strong as to push events beyond the bounds of natural variability alone. It was also predicted that we would first observe this phenomenon for heat events where the climate change influence is most pronounced. Additional retrospective analysis will reveal if, in fact, these are the first events of their kind or were simply some of the first to be discovered.

Last year, the editors emphasized the need for additional papers in the area of "impacts attribution" that investigate whether climate change's influence on the extreme event can subsequently be directly tied to a change in risk of the socio-economic or environmental impacts. Several papers in this year's report address this challenge, including Great Barrier Reef bleaching, living marine resources in the Pacific, and ecosystem productivity on the Iberian Peninsula. This is an increase over the number of impact attribution papers than in the past, and are hopefully a sign that research in this area will continue to expand in the future.

Other extreme weather event types in this year's edition include ocean heat waves, forest fires, snow storms, and frost, as well as heavy precipitation, drought, and extreme heat and cold events over land. There were a number of marine heat waves examined in this year's report, and all but one found a role for climate change in increasing the severity of the events. While human-caused climate change caused China's cold winter to be less likely, it did not influence U.S. storm Jonas which hit the mid-Atlantic in winter 2016.

As in past years, the papers submitted to this report are selected prior to knowing the final results of whether human-caused climate change influenced the event. The editors have and will continue to support the publication of papers that find no role for human-caused climate change because of their scientific value in both assessing attribution methodologies and in enhancing our understanding of how climate change is, and is not, impacting extremes. In this report, twenty-one of the twenty-seven papers in this edition identified climate change as a significant driver of an event, while six did not. Of the 131 papers now examined in this report over the last six years, approximately 65% have identified a role for climate change, while about 35% have not found an appreciable effect.

Looking ahead, we hope to continue to see improvements in how we assess the influence of human-induced climate change on extremes and the continued inclusion of stakeholder needs to inform the growth of the field and how the results can be applied in decision making. While it represents a considerable challenge to provide robust results that are clearly communicated for stakeholders to use as part of their decision-making processes, these annual reports are increasingly showing their potential to help meet such growing needs.

4. THE EXTREME 2015/16 EL NIÑO, IN THE CONTEXT OF HISTORICAL CLIMATE VARIABILITY AND CHANGE

Matthew Newman, Andrew T. Wittenberg, Linyin Cheng, Gilbert P. Compo, and Catherine A. Smith

Record warm central equatorial Pacific Ocean temperatures during the 2015/16 El Niño appear to partly reflect an anthropogenically forced trend. Whether they reflect changes in El Niño variability remains uncertain.

Introduction. Recent studies have investigated whether both the amplitude and key characteristics of El Niño–Southern Oscillation (ENSO) events have been changing, potentially due to some natural and/or anthropogenic change in the tropical Pacific Ocean state during recent decades (e.g., Yeh et al. 2009; Lee and McPhaden 2010; Newman et al. 2011; McGregor et al. 2013). If so, when might this change be identifiable in individual ENSO events? Was the extreme warmth in the equatorial Pacific seen in the recent 2015/16 El Niño, particularly near the dateline (L'Heureux et al. 2017), a harbinger of this change? To address these questions, we assess this event using statistics of Niño3 (5°N–5°S, 150°–90°W) and Niño4 (5°N–5°S, 160°E–150°W) sea surface temperature (SST) indices, derived from observational datasets and coupled general circulation model simulations. We use two indices to capture differences between events, important to both forecasts and diagnosis of ENSO and its impacts (Compo and Sardeshmukh 2010; Capotondi et al. 2015).

How extreme was the 2015/16 El Niño? We compare the December 2015 (DEC2015) equatorial SST anomaly (SSTA) to the SSTA distribution during 1891–2000, to more stringently test against potentially recent nonstationarity. (Other winter months yielded similar results.) Figure 4.1 shows histograms of monthly ERSST.v5 Niño3 and Niño4 indices, compared with two different probability distribution functions (PDFs) determined not by fitting the histogram, but by fitting two different Markov processes to each index time series: an AR1 process (or red noise; e.g., Frankignoul and Hasselmann 1977) with a memory time scale on the order of several months, yielding a Gaussian (normal) distribution; and a "stochastically generated skewed" process (SGS; Sardeshmukh et al. 2015), similar to the AR1 process but with noise that is asymmetric and depends linearly on the SSTA, yielding a non-Gaussian (skewed and heavy-tailed) distribution. Confidence intervals for these PDFs are determined from large ensembles of 110-year realizations generated by each process. (See online supplement for details.)

The SGS distribution captures the significant positive skewness of the Niño3 PDF (Fig. 4.1a). The observed tail probability (the probability of Niño3 reaching its observed DEC2015 magnitude) is underestimated by the Gaussian AR1 PDF, but not by the skewed SGS PDF. This result is insensitive to the dataset or to removing the 1891–2015 linear trend. Overall, the SGS distributions suggest that the probability of a monthly Niño3 value reaching or exceeding the DEC2015 magnitude is about 0.5%, consistent with previous occurrences of strong El Niño events in the observational record.

Results are quite different for Niño4, where weak negative skewness (Fig. 4.1b) means that the Gaussian distribution overestimates the DEC2015 tail probability. The DEC2015 Niño4 value was unprecedented in all five datasets, apparently impacted by a secular warming trend. Relative to its linear trend, however, the ERSST.v5 dataset had higher Niño4 values earlier in the record.

How likely was the 2015/16 El Niño? We next evaluate the likelihood and severity of the 2015/16 event relative to the gradually warming background by applying the generalized extreme value (GEV) distribution (e.g., Coles 2001; Ferreira and de Haan

AFFILIATIONS: Newman, Cheng, Compo, and Smith—CIRES, University of Colorado, Boulder, and NOAA Earth Systems Research Laboratory, Physical Sciences Division, Boulder, Colorado; Wittenberg—NOAA Geophysical Fluid Dynamics Laboratory, Princeton, New Jersey

DOI:10.1175/BAMS-D-17-0116.1

A supplement to this article is available online (10.1175/BAMS-D-17-0116.2)

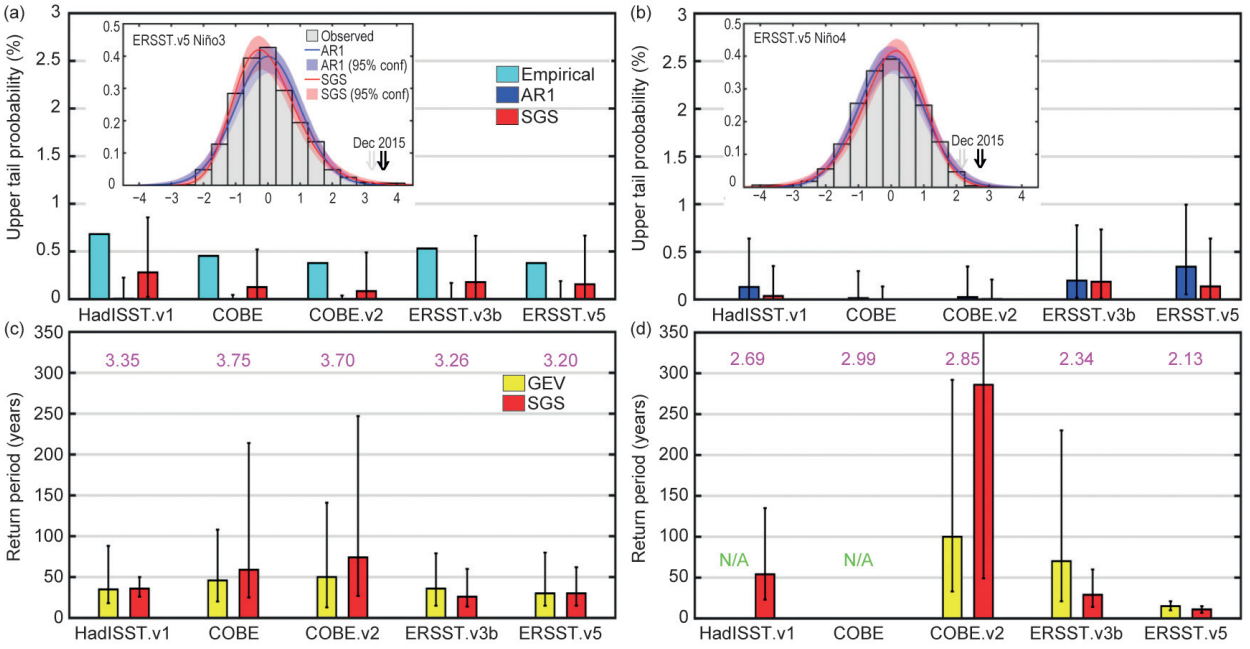

Fig. 4.1. Estimations of DEC2015 (a) Niño3 and (b) Niño4 upper tail probabilities (%). For each SST reconstruction, bars show the scalar tail probability empirically derived from the dataset and also its median value from AR1 and SGS distributions; ranges are shown by the whiskers. Insets compare SGS and AR1 PDFs with data histograms, using ERSST.v5 values standardized with respect to 1891–2000 (other datasets yielded similar results). Corresponding 95% confidence intervals are shaded; DEC2015 amplitudes are indicated by arrows, where the linear trend is (gray) or is not (black) first removed. Return period estimation (years) of linearly detrended 2015/16 (c) Niño3 and (d) Niño4 indices using the annual maximum of monthly SSTs. For each SST reconstruction, the bars show the 110-year sampling distribution of the return period matching the observed 2015/16 standardized values (magenta numbers), with ranges shown by the whiskers. N/A indicates return periods not derivable using the GEV technique (see text).

2015) to the historical annual maximum of linearly detrended monthly Niño3 and Niño4 indices during 1891–2000. [See online supplement for our Bayesian analysis (Cheng et al. 2014).] The return period, or (re) occurrence probability of an El Niño event with the observed 2015/16 intensity (a "2015/16-level" event), is derived for both indices from each dataset. The same assessment is repeated with the SGS ensembles discussed above.

Our analysis suggests that a 2015/16-level event could be expected for Niño3 roughly once every 40 years. This median return period is reasonably robust to the observational or synthetic SGS dataset used. However, the uncertainty estimates for the return period, and thus the likelihood of the 2015/16 event, are less robust. Both ERSST datasets showed the least uncertainty and shortest return periods, with a 2015/16-level Niño3 SSTA occurring every 5 to 50 years, while COBE2 showed the greatest uncertainty with a range of 10 to 120 years. The SGS distributions, which have more extreme tail events, reduced the return period uncertainty for the ERSST and HadISST.v1 datasets and suggested a greater likelihood of 2015/16-level SSTA extremes.

For Niño4, there is much less agreement among the datasets (Fig. 4.1d), with the return period of a 2015/16-level event lowest for the ERSST datasets. For those datasets where the 2015/16 Niño4 SSTA was unprecedented, the return period cannot be derived using the GEV approach. From ERSST.v5, however, such an event could occur one year in ten.

Was the 2015/16 El Niño impacted by multidecadal trends in equatorial Pacific SST or ENSO variability? Figure 4.2 illustrates the evolution of 30-year mean SST and 30-year ENSO amplitude over the past 160 years, for two observational reconstructions and two model simulations. For simplicity we discuss only the HadISST.v1.1 and ERSST.v5 reconstructions, which generally bound the behavior of the other products we examined (HadISST.v2, ERSST.v3b, ERSST.v4, COBE, COBE.v2, Kaplan.v2, SODA-si.v3).

For both Niño3 and Niño4, the 1987–2016 epoch was observed to be either the warmest or the second

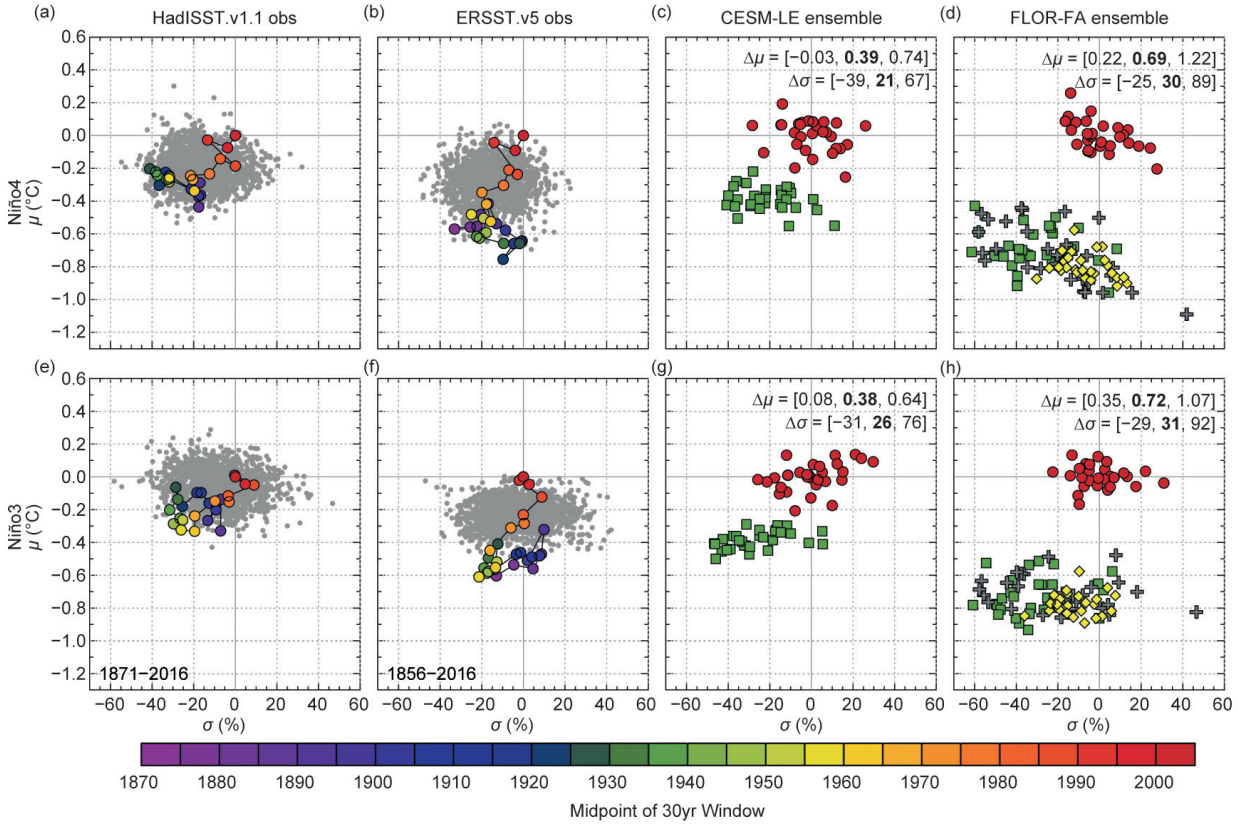

Fig. 4.2. Statistics for annually smoothed SSTs averaged over (a)–(d) Niño4 and (e)–(h) Niño3. Y-axis is the 30-year mean (μ, °C departure from 1987–2016); x-axis is the 30-year std dev (σ, % departure from 1987–2016). (a),(b),(e),(f) sample the observationally reconstructed 30-year statistics every 5 years (colored dots). Gray dots show analogous statistics from 8000-year LIM simulations trained using detrended 1959–2000 data from HadISST.v1.1 or ERSST.v5. (c),(g) show the CESM-LE 30-member ensemble simulation with "ALL" (anthropogenic + natural) historical forcings, for 1987–2016 (red dots) and 1920–49 (green squares) relative to the 1987–2016 ensemble mean; inset indicates ALL ensemble [minimum, average, maximum] change in μ and σ from 1920–49 to 1987–2016. (d),(h) show analogous statistics for the FLOR-FA 30-member ALL ensemble, along with a 30-member "NAT" ensemble with natural forcings only for 1920–49 (gray crosses) and 1987–2016 (yellow diamonds), also relative to the ALL ensemble mean.

warmest 30-year epoch on record, depending on the observational dataset. The warming trend is clearest after 1970 and in Niño4. It is more pronounced in ERSST.v5 than HadISST.v1.1. The centennial warming of both indices is marginally within the bounds of what could be expected from intrinsic multidecadal variations for HadISST.v1.1, but is outside the bounds for ERSST.v5, relative to a statistically stationary multivariate AR1 process [a linear inverse model (LIM), constructed from detrended observed tropical SSTAs during 1959–2000; see online supplement and Newman et al. 2011]. This is consistent with earlier analysis (Solomon and Newman 2012) finding equatorial Pacific 1900–2010 warming trends to be significant near and west of the dateline, despite uncertainty in amplitude.

Robust equatorial Pacific warming from 1920–49 to 1987–2016 is evident in ensemble simulations from the NCAR CESM-LE and GFDL FLOR-FA global coupled GCMs driven by historical natural and anthropogenic ("ALL") forcings (Figs. 4.2c,d,g,h). CESM-LE's warming is compatible with all the reconstructions, though most of its members warm more than HadISST.v1.1 and less than ERSST.v5. FLOR-FA's warming is strong enough to be detected with any pair of 30-year means drawn randomly from each epoch. It is marginally compatible with ERSST.v5 but not with HadISST.v1.1. The FLOR-FA ensemble simulation with only natural (solar and volcanic, "NAT") forcings shows ensemble-mean cooling from 1920–49 to 1987–2016, so the FLOR-FA ALL warming must be entirely anthropogenic.

Compared to the historical changes in 30-year mean SST, there is less observational consensus about changes in ENSO SSTA variance. In Niño4, HadISST.v1.1 shows a fairly monotonic 40% amplifi-

cation of ENSO from the 1920s to the present, while ERSST.v5 shows only a 10% amplification and more interdecadal modulation of ENSO amplitude; neither exceeds the expected bounds of intrinsic multidecadal variations. In Niño3, ENSO amplitudes strengthen by 10% in HadISST.v1.1 since 1900, but weaken by 10% in ERSST.v5.

The CESM-LE and FLOR-FA ALL simulations both show ensemble-mean ENSO amplification from 1920–49 to 1987–2016. However, the strong intrinsic interdecadal modulation of ENSO means that some individual realizations experience greater or smaller amplification; a few even weaken. The simulations are broadly consistent with the reconstructed historical changes in ENSO amplitude, but this is primarily due to the reconstruction uncertainty and to intrinsic modulation of ENSO that produces large sampling variability of amplitudes over 30-year epochs (Wittenberg 2009; Newman et al. 2011). Interestingly, the FLOR-FA ALL and NAT simulations both show ENSO amplification (and reduced ENSO modulation) during 1987–2016, mainly because the quietest epochs vanish, suggesting natural forcings are key to the FLOR-FA results.

Conclusions. The 2015/16 El Niño was a strong but not unprecedented warm event in the eastern equatorial Pacific (Niño3), comparable to events occurring every few decades or so. However, central equatorial Pacific (Niño4) 2015/16 warmth was unprecedented in all SST reconstruction datasets except ERSST.v4. This exceptional warmth was unlikely, although not impossible, to have occurred entirely naturally, and appears to reflect an anthropogenically forced trend.

Whether this extreme warmth was associated with a change in ENSO variability, however, is less clear, given the substantial disagreement between datasets including uncertainty in their anthropogenic trend estimates (Deser et al. 2010; Solomon and Newman 2012). Interestingly, SST reconstructions with relatively higher Niño3 and Niño4 variances around the start of the 20th century (e.g., ERSST.v5) are also based on newer ICOADS releases, which include additional observations during that time (Freeman et al. 2016). Moreover, equatorial Pacific sea level pressure variance (i.e., Darwin and Tahiti) shows no pronounced centennial increase (e.g., Torrence and Compo 1998). Finally, our model results illuminate, but do not reconcile, continuing disparities among climate models concerning anthropogenic impacts on ENSO variability (Collins et al. 2010; Watanabe et al. 2012; Capotondi et al. 2015) due to lingering dynamical biases in the models (Bellenger et al. 2014; Graham et al. 2017). These issues suggest that we cannot yet confidently detect whether a secular change in ENSO variability (apart from the background warming) has occurred over the past century. Our study thus highlights the need to further reduce uncertainty in observational reconstructions, and further improve dynamical models, to better gauge future ENSO risks.

REFERENCES

Bellenger, H., E. Guilyardi, J. Leloup, M. Lengaigne, and J. Vialard, 2014: ENSO representation in climate models: From CMIP3 to CMIP5. *Climate Dyn.,* **42**, 1999–2018, doi:10.1007/s00382-013-1783-z.

Capotondi, A., and Coauthors, 2015: Understanding ENSO diversity. *Bull. Amer. Meteor. Soc.*, **96**, 921–938, doi:10.1175/BAMS-D-13-00117.1.

Cheng, L., A. AghaKouchak, E. Gilleland, and R. W. Katz, 2014: Non-stationary extreme value analysis in a changing climate. *Climatic Change*, **127**, 353–369, doi:10.1007/s10584-014-1254-5.

Coles, S., 2001: *An Introduction to Statistical Modeling of Extreme Values*. Springer, 209 pp.

Collins, M., and Coauthors, 2010: The impact of global warming on the tropical Pacific Ocean and El Niño. *Nat. Geosci.*, **3**, 391–397, doi:10.1038/ngeo868.

Compo, G. P., and P. D. Sardeshmukh, 2010: Removing ENSO-related variations from the climate record. *J. Climate*, **23**, 1957–1978, doi:10.1175/2009JCLI2735.1.

Deser, C., A. S. Phillips, and M. A. Alexander, 2010: Twentieth century tropical sea surface temperature trends revisited. *Geophys. Res. Lett.*, **37**, L10701, doi:10.1029/2010GL043321.

Ferreira, A., and L. de Haan, 2015: On the block maxima method in extreme value theory: PWM estimators. *Annals of Statistics*, **43**, 276–298, doi:10.1214/14-AOS1280.

Frankignoul, C., and K. Hasselmann, 1977: Stochastic climate models. Part II: Application to sea-surface temperature anomalies and thermocline variability. *Tellus A*, **29**, 289–305.

Freeman, E., and Coauthors, 2016: ICOADS Release 3.0: A major update to the historical marine climate record. *Int. J. Climatol.*, **37**, 2211–2232, doi:10.1002/joc.4775.

Graham, F. S., A. T. Wittenberg, J. N. Brown, S. J. Marsland, and N. J. Holbrook, 2017: Understanding the double peaked El Niño in coupled GCMs. *Climate Dyn.*, **48**, 2045–2063, doi:10.1007/s00382-016-3189-1.

L'Heureux, M. L., and Coauthors, 2017: Observing and predicting the 2015/16 El Niño. *Bull. Amer. Meteor. Soc.*, **98**, 1363–1382, doi:10.1175/BAMS-D-16-0009.1.

Lee, T., and M. J. McPhaden, 2010: Increasing intensity of El Niño in the central-equatorial Pacific. *Geophys. Res. Lett.,* **37**, L14603, doi:10.1029/2010GL044007.

McGregor, S., A. Timmermann, M. H. England, O. Elison Timm, and A. T. Wittenberg, 2013: Inferred changes in El Niño–Southern Oscillation variance over the past six centuries. *Climate Past*, **9**, 2269–2284, doi:10.5194/cp-9-2269-2013.

Newman, M., S.-I. Shin, and M. A. Alexander, 2011: Natural variation in ENSO flavors. *Geophys. Res. Lett.,* **38**, L14705, doi:10.1029/2011GL047658.

Sardeshmukh, P. D., G. P. Compo, and C. Penland, 2015: Need for caution in interpreting extreme weather statistics. *J. Climate*, **28**, 9166–9187, doi:10.1175/JCLI-D-15-0020.1.

Solomon, A., and M. Newman, 2012: Reconciling disparate twentieth-century Indo-Pacific ocean temperature trends in the instrumental record. *Nat. Climate Change*, **2**, 691–699, doi:10.1038/nclimate1591.

Torrence, C., and G. P. Compo, 1998: A practical guide to wavelet analysis. *Bull. Amer. Meteor. Soc*. **79**, 61–78, doi:10.1175/15200477(1998)079<0061:APGTWA>2.0.CO;2.

Watanabe, M., J.-S. Kug, F.-F. Jin, M. Collins, M. Ohba, and A. T. Wittenberg, 2012: Uncertainty in the ENSO amplitude change from the past to the future. *Geophys. Res. Lett.*, **39**, L20703, oi:10.1029/2012GL053305.

Wittenberg, A. T., 2009: Are historical records sufficient to constrain ENSO simulations? *Geophys. Res. Lett*., **36**, L12702, doi:10.1029/2009GL038710.

Yeh, S.-W. J.S. Kug, B. Dewitte, M.-H. Kwon, B. P. Kirtman, and F.F. Jin, 2009: El Niño in a changing climate. *Nature*, **461**, 511–514, doi:10.1038/nature08316

Table 1.1. SUMMARY of RESULTS

ANTHROPOGENIC INFLUENCE ON EVENT			
	INCREASE	**DECREASE**	**NOT FOUND OR UNCERTAIN**
Heat	Ch. 3: Global Ch. 7: Arctic Ch. 15: France Ch. 19: Asia		
Cold		Ch. 23: China Ch. 24: China	
Heat & Dryness	Ch. 25: Thailand		
Marine Heat	Ch. 4: Central Equatorial Pacific Ch. 5: Central Equatorial Pacific Ch. 6: Pacific Northwest Ch. 8: North Pacific Ocean/Alaska Ch. 9: North Pacific Ocean/Alaska Ch. 9: Australia		Ch. 4: Eastern Equatorial Pacific
Heavy Precipitation	Ch. 20: South China Ch. 21: China (Wuhan) Ch. 22: China (Yangtze River)		Ch. 10: California (failed rains) Ch. 26: Australia Ch. 27: Australia
Frost	Ch. 29: Australia		
Winter Storm			Ch. 11: Mid-Atlantic U.S. Storm "Jonas"
Drought	Ch. 17: Southern Africa Ch. 18: Southern Africa		Ch. 13: Brazil
Atmospheric Circulation			Ch. 15: Europe
Stagnant Air			Ch. 14: Western Europe
Wildfires	Ch. 12: Canada & Australia (Vapor Pressure Deficits)		
Coral Bleaching	Ch. 5: Central Equatorial Pacific Ch. 28: Great Barrier Reef		
Ecosystem Function		Ch. 5: Central Equatorial Pacific (Chl-***a*** and primary production, sea bird abundance, reef fish abundance) Ch. 18: Southern Africa (Crop Yields)	
El Niño	Ch. 18: Southern Africa		Ch. 4: Equatorial Pacific (Amplitude)
TOTAL	18	3	9

	METHOD USED	Total Events
Heat	Ch. 3: CMIP5 multimodel coupled model assessment with piCont, historicalNat, and historical forcings Ch. 7: CMIP5 multimodel coupled model assessment with piCont, historicalNat, and historical forcings Ch. 15: Flow analogues conditional on circulation types Ch. 19: MIROC-AGCM atmosphere only model conditioned on SST patterns	
Cold	Ch. 23: HadGEM3-A (GA6) atmosphere only model conditioned on SST and SIC for 2016 and data fitted to GEV distribution Ch. 24: CMIP5 multimodel coupled model assessment	
Heat & Dryness	Ch. 25: HadGEM3-A N216 Atmosphere only model conditioned on SST patterns	
Marine Heat	Ch. 4: SST observations; SGS and GEV distributions; modeling with LIM and CGCMs (NCAR CESM-LE and GFDL FLOR-FA) Ch. 5: Observational extrapolation (OISST, HadISST, ERSST v4) Ch. 6: Observational extrapolation; CMIP5 multimodel coupled model assessment Ch. 8: Observational extrapolation; CMIP5 multimodel coupled model assessment Ch. 9: Observational extrapolation; CMIP5 multimodel coupled model assessment	
Heavy Precipitation	Ch. 10: CAM5 AMIP atmosphere only model conditioned on SST patterns and CESM1 CMIP single coupled model assessment Ch. 20: Observational extrapolation; CMIP5 and CESM multimodel coupled model assessment; auto-regressive models Ch. 21: Observational extrapolation; HadGEM3-A atmosphere only model conditioned on SST patterns; CMIP5 multimodel coupled model assessment with ROF Ch. 22: Observational extrapolation, CMIP5 multimodel coupled model assessment Ch. 26: BoM seasonal forecast attribution system and seasonal forecasts Ch. 27: CMIP5 multimodel coupled model assessment	
Frost	Ch. 29: *weather@home* multimodel atmosphere only models conditioned on SST patterns; BoM seasonal forecast attribution system	
Winter Storm	Ch. 11: ECHAM5 atmosphere only model conditioned on SST patterns	
Drought	Ch. 13: Observational extrapolation; weather@home multimodel atmosphere only models conditioned on SST patterns; HadGEM3-A and CMIP5 multimodel coupled model assessent; hydrological modeling Ch. 17: Observational extrapolation; CMIP5 multimodel coupled model assessment; VIC land surface hdyrological model, optimal fingerprint method Ch. 18: Observational extrapolation; *weather@home* multimodel atmosphere only models conditioned on SSTs, CMIP5 multimodel coupled model assessment	
Atmospheric Circulation	Ch. 15: Flow analogues distances analysis conditioned on circulation types	
Stagnant Air	Ch. 14: Observational extrapolation; Multimodel atmosphere only models conditioned on SST patterns including: HadGEM3-A model; EURO-CORDEX ensemble; EC-EARTH+RACMO ensemble	
Wildfires	Ch. 12: HadAM3 atmospere only model conditioned on SSTs and SIC for 2015/16	
Coral Bleaching	Ch. 5: Observations from NOAA Pacific Reef Assessment and Monitoring Program surveys Ch. 28: CMIP5 multimodel coupled model assessment; Observations of climatic and environmental conditions (NASA GES DISC, HadCRUT4, NOAA OISSTV2)	
Ecosystem Function	Ch. 5: Observations of reef fish from NOAA Pacific Reef Assessment and Monitoring Program surveys; visual observations of seabirds from USFWS surveys. Ch. 18: Empirical yield/rainfall model	
El Niño	Ch. 4: SST observations; SGS and GEV distributions; modeling with LIM and CGCMs (NCAR CESM-LE and GFDL FLOR-FA) Ch. 18: Observational extrapolation; *weather@home* multimodel atmosphere only models conditioned on SSTs, CMIP5 multimodel coupled model assessment	
		30